Upper Mantle Seismic Anisotropy beneath the Northern Transantarctic Mountains, Antarctica from PKS, SKS, and SKKS Splitting Analysis

Jordan H. Graw – The University of Alabama
Samantha E. Hansen – The University of Alabama

Citation of published version:
Graw, J., Hansen, S. (2017): Upper Mantle Seismic Anisotropy beneath the Northern Transantarctic Mountains, Antarctica from PKS, SKS, and SKKS Splitting Analysis. *Geochemistry, Geophysics, Geosystems,* 18(2).
DOI: https://doi.org/10.1002/2016GC006729

AGU PUBLICATIONS

Geochemistry, Geophysics, Geosystems

RESEARCH ARTICLE
10.1002/2016GC006729

Key Points:
- Shear-wave splitting analysis is used to determine anisotropic parameters for individual stations within Northern Victoria Land, Antarctica
- Results show two distinct geographic regions of anisotropy
- Anisotropy in East Antarctica reflects relict fabric in the lithosphere, while anisotropy along the coast reflects active upper mantle flow

Supporting Information:
- Supporting Information S1

Correspondence to:
J. H. Graw,
jhgraw@crimson.ua.edu

Citation:
Graw, J. H., and S. E. Hansen (2017), Upper mantle seismic anisotropy beneath the Northern Transantarctic Mountains, Antarctica from PKS, SKS, and SKKS splitting analysis, *Geochem. Geophys. Geosyst.*, *18*, 544–557, doi:10.1002/2016GC006729.

Received 14 NOV 2016
Accepted 20 JAN 2017
Accepted article online 28 JAN 2017
Published online 12 FEB 2017

Upper mantle seismic anisotropy beneath the Northern Transantarctic Mountains, Antarctica from PKS, SKS, and SKKS splitting analysis

Jordan H. Graw[1] and Samantha E. Hansen[1]

[1]Department of Geological Sciences, The University of Alabama, Tuscaloosa, Alabama, USA

Abstract Using data from the new Transantarctic Mountains Northern Network, this study aims to constrain azimuthal anisotropy beneath a previously unexplored portion of the Transantarctic Mountains (TAMs) to assess both past and present deformational processes occurring in this region. Shear-wave splitting parameters have been measured for PKS, SKS, and SKKS phases using the eigenvalue method within the SplitLab software package. Results show two distinct geographic regions of anisotropy within our study area: one behind the TAMs front, with an average fast axis direction of 42 ± 3° and an average delay time of 0.9 ± 0.04 s, and the other within the TAMs near the Ross Sea coastline, with an average fast axis oriented at 51 ± 5° and an average delay time of 1.5 ± 0.08 s. Behind the TAMs front, our results are best explained by a single anisotropic layer that is estimated to be 81–135 km thick, thereby constraining the anisotropic signature within the East Antarctic lithosphere. We interpret the anisotropy behind the TAMs front as relict fabric associated with tectonic episodes occurring early in Antarctica's geologic history. For the coastal stations, our results are best explained by a single anisotropic layer estimated to be 135–225 km thick. This places the anisotropic source within the viscous asthenosphere, which correlates with low seismic velocities along the edge of the West Antarctic Rift System. We interpret the coastal anisotropic signature as resulting from active mantle flow associated with rift-related decompression melting and Cenozoic extension.

1. Introduction

The Transantarctic Mountains (TAMs; Figure 1), which span a length of ~3500 km, reach elevations of ~4500 m, and separate the East Antarctica craton from the West Antarctic Rift System (WARS), are the largest noncompressional mountain chain on Earth [*Robinson and Splettstoesser*, 1984]. Despite their relatively simple stratigraphy, the tectonic history of the TAMs is complex, and their associated uplift mechanism is largely unconstrained. Precambrian igneous and metamorphic rocks associated with the Nimrod and Beardmore Orogenies compose the oldest strata within the TAMs (Figure 1) [*ten Brink et al.*, 1997; *Goodge et al.*, 2001]. In the Late Cambrian (~500 Ma), East Antarctica acted as the overriding tectonic plate in a subduction zone that paralleled the present-day TAMs during the Ross Orogeny and during the final amalgamation of Gondwanaland [*Dalziel*, 1992], leading to metasedimentary strata and Cambrian-Ordovician granites. This subductional margin migrated seaward with the accretion of new terranes, and a transition to transpressional motion occurred through the Paleozoic [*Fitzgerald*, 2002]. Between the Ordovician and Devonian, the basement rocks were exhumed, and a distinct erosional surface known as the Kukri Peneplain developed (Figure 1). The peneplain uncomformably separates the basement rocks from the overlying Devonian to Triassic Beacon Supergroup, a subhorizontal sedimentary sequence with a shallow marine and fluvial origin [*Barrett*, 1991]. Both the basement and the Beacon strata are intruded by dolerite dikes and sills of the Ferrar Supergroup and are overlain by the Kirkpatrick basalt, a short-lived continental flood basalt province associated with initial supercontinent breakup in the Jurassic. However, following the Mesozoic magmatism, the on-land geologic record within the TAMs has a ~160 Ma gap. Inferences of post-Jurassic tectonic movement have been made using the older geologic units. More specifically, the Jurassic sills and basalts, the Beacon sediments, and the Kukri Peneplain show no evidence for folding or reverse faulting, indicating the lack of a compressional tectonic event between the Mesozoic and the present day. The youngest rocks in the TAMs are Neogene volcanics composing the McMurdo Volcanic Group, which can be dated to ~19 Ma [*Fitzgerald et al.*, 1986; *Kyle and Muncy*, 1989].

Given the large gap in the geologic record, there are many questions about the timing and extent of the TAMs uplift, and several approaches have been taken to constrain these characteristics. For instance, apatite

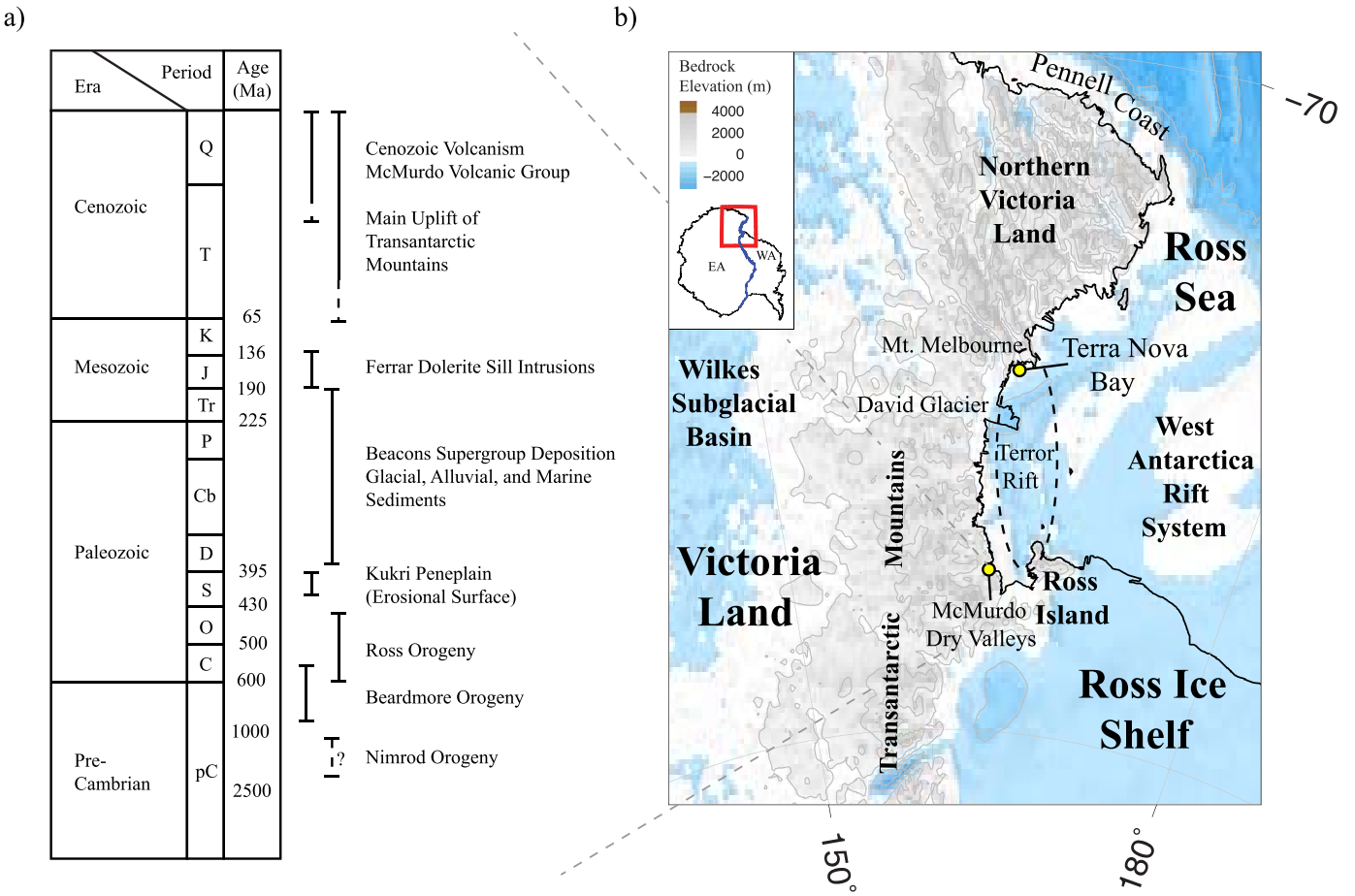

Figure 1. Geologic overview of the study area. (a) Simplified stratigraphic column, highlighting the events associated with the tectonic history of the TAMs [*Kalamarides et al.*, 1987]. (b) Map of the study area, indicating key features referenced in the text. Topographic bedrock elevations are from the BEDMAP2 model [*Fretwell et al.*, 2013]. (inset) Outline of Antarctica with the study area highlighted by the red box. The blue line shows the boundary where East Antarctica (EA) meets West Antarctica (WA).

fission track analysis chronicles three main phases of exhumation: Early Cretaceous, Late Cretaceous, and Early Cenozoic, with the most significant exhumation of ∼6 km occurring at ∼55 Ma [*Fitzgerald et al.*, 1986; *Fitzgerald*, 2002]. The fission track uplift estimate is supported by stratigraphic evidence. At ∼80 Ma, the Kukri Peneplain had to be buried at a depth of ∼4 km [*Lisker and Läufer*, 2013]; however, today it can be found at elevations of 500–4000 m above sea level [*Fitzgerald and Stump*, 1997]. The lack of compressional structures in the TAMs has led to a number of alternative uplift mechanisms being proposed. These include thermal buoyancy from hotter upper mantle beneath the WARS and flexural uplift [*Stern and ten Brink*, 1989; *ten Brink et al.*, 1997], basin subsidence and rift flank uplift with the inclusion of a crustal root beneath the TAMs [*Studinger et al.*, 2004; *Karner et al.*, 2005], which may have been generated by the extensional collapse of thickened crust beneath West Antarctica [*Bialas et al.*, 2007; *Huerta and Harry*, 2007], or a hybrid model of the aforementioned including a combination of erosional unloading, local crustal isostasy, and thermal buoyancy [*Lawrence et al.*, 2006a].

The tectonic structure of the TAMs, and its relation to their geologic history and potential uplift mechanism, has been investigated by a number of previous seismic studies, primarily focused on tomographic imaging and receiver function analyses [e.g., *Watson et al.*, 2006; *Lawrence et al.*, 2006a, 2006b; *Hansen et al.*, 2009, 2016; *Brenn,* 2016; *Graw et al.*, 2016]. However, additional characterization of this dynamic environment can be obtained by examining the anisotropic signature of this area [*Pondrelli et al.*, 2005; *Barklage et al.*, 2009; *Salimbeni et al.*, 2010]. Seismically anisotropic layers cause incoming *S* waves to split into two orthogonal components, one traveling faster than the other. The anisotropy can be characterized by the azimuth of the polarization plane of the faster *S* wave (i.e., the fast axis, φ) and the delay time (δt) between the two

orthogonal components [*Silver and Chan*, 1991]. Generally, seismic anisotropy is attributed to the lattice preferred orientation (LPO) of olivine crystals in the upper mantle, where φ is aligned parallel to the dominant shear strain direction [*Silver and Chan*, 1988; *Fischer et al*., 1998]. LPO develops through tectonic deformation; therefore, the associated φ may either reflect present-day mantle flow, associated with absolute plate motion (APM) or with tectonic forces, or it may reflect past deformational episodes that have been "frozen" as relict fabric in the lithosphere [*Zhang et al*., 2000; *Mainprice et al*., 2005]. The δt between the fast and slow waves is associated with the percentage or magnitude of anisotropy as well as the thickness of the anisotropic layer.

Using data from a new array of seismic stations, the goal of the current study is to measure the seismic anisotropy beneath the TAMs in Northern Victoria Land, particularly in relation to the mantle velocity structure imaged beneath this region [*Graw et al*., 2016; *Brenn*, 2016]. By measuring shear-wave splitting parameters (φ and δt), we will better constrain the deformation processes and tectonic fabric in the northern TAMs, ultimately providing improved constraints on the geologic history of this enigmatic region.

2. Previous Seismological Investigations

2.1. Crustal and Upper Mantle Structure: Tomography and Receiver Function Constraints

Both continental-scale and global-scale tomographic models highlight two seismically distinct regions beneath Antarctica: East Antarctica, which is underlain by seismically fast velocities typical of cratonic environments, and West Antarctica, which is underlain by seismically slow velocities and has been interpreted as a region of extension and volcanism (Figure 1) [*Ritzwoller et al*., 2001; *Sieminski et al*., 2003; *Morelli and Danesi*, 2004; *Hansen et al*., 2014]. Average crustal thickness across East Antarctica is 35–45 km [*Ritzwoller et al*., 2001; *Hansen et al*., 2009, 2010], while the crustal thickness beneath West Antarctica is much thinner, averaging ~27 km [*Ritzwoller et al*., 2001; *Chaput et al*., 2014; *Heeszel et al*., 2016]. Additionally, the lithospheric thickness beneath East Antarctica is also greater, reaching a maximum thickness of ~250 km [*Morelli and Danesi*, 2004], while that beneath West Antarctica is much thinner, ranging from ~60 km in the Terror Rift area (Figure 1) to 70–100 km beneath the eastern Ross Sea and inner WARS [*Huerta*, 2007; *Heeszel et al*., 2016]. The TAMs overlie the boundary between these two tectonic regimes.

Much of our knowledge about the crustal and upper mantle structure beneath the TAMs comes from regional seismic investigations. For instance, the Transantarctic Mountains Seismic Experiment (TAMSEIS; Figure 2) operated within the central TAMs near Ross Island from November 2000 to December 2003. Crustal thickness estimates from TAMSEIS generally show thickening from the Ross Sea coast inland, changing from ~20 to 35–40 km over a lateral distance of about 80–100 km [*Lawrence et al*., 2006a, 2006b; *Hansen et al*., 2009]. Additionally, the crustal thickness behind the TAMs front and within East Antarctica is comparable to that found beneath the mountain range [*Hansen et al*., 2009], and this characteristic has been used to argue that crustal buoyancy is likely only a minor factor contributing to the TAMs' uplift. *P* and *S* wave tomography models [*Watson et al*., 2006] as well as surface wave phase velocity analyses [*Lawrence et al*., 2006b] based on the TAMSEIS data highlight fast seismic velocities (~4.5 km s^{-1}) beneath East Antarctica and anomalously slow (~4.2 km s^{-1}) upper mantle velocities beneath Ross Island. These slow velocities extend 50–100 km inland beneath the McMurdo Dry Valleys region of the TAMs (Figure 1) and are restricted to upper mantle depths (<~200 km). The tomographic studies attribute the slow seismic anomalies to hot upper mantle material beneath the WARS and suggest that thermal buoyancy significantly contributes to uplift in the central TAMs, which is consistent with the flexural origin model proposed by *Stern and ten Brink* [1989] and *ten Brink et al*. [1997]. However, both the *Watson et al*. [2006] and *Lawrence et al*. [2006b] models lose resolution north of Ross Island, calling the along-strike structure beneath the TAMs into question and spurring the need for further analysis along the mountain range.

More recently, the Transantarctic Mountains Northern Network (TAMNNET) was deployed in Northern Victoria Land to expand seismic investigations of the TAMs (Figure 2) [*Hansen et al*., 2015]. Similar to TAMSEIS, little evidence for a thick crustal root is observed beneath the TAMNNET array [*Hansen et al*., 2016]. Further, both surface [*Graw et al*., 2016] and body wave [*Brenn*, 2016] tomography models generated with the TAMNNET data indicate a previously unidentified low velocity anomaly beneath the northern TAMs. Similar to the Ross Island region, the slow velocities are primarily constrained above ~200 km depth in the vicinity of Mt. Melbourne (Figure 1), and they extend inland beneath the TAMs front. Additionally,

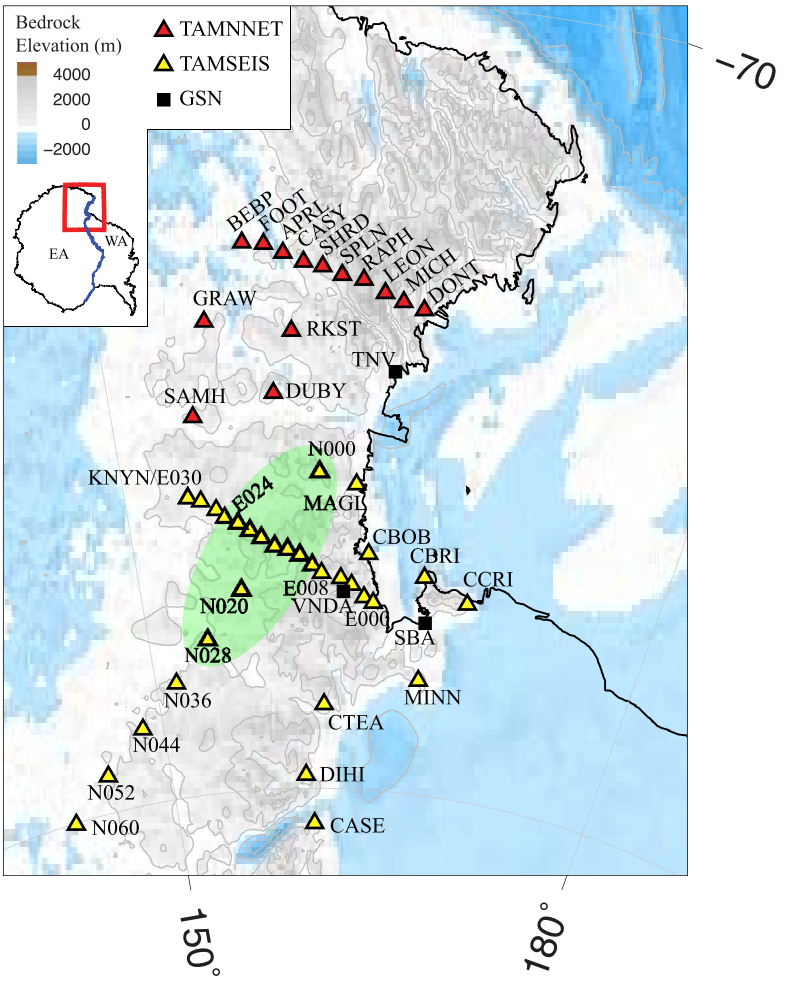

Figure 2. Map showing the seismic stations from this study as well as from some previous studies. TAMNNET stations are represented by red triangles, TAMSEIS stations are yellow triangles, and GSN stations are black squares. The green shaded area encompasses the stations used for anisotropic analyses by *Lawrence et al.* [2006b]. Topographic bedrock elevations are from the BEDMAP2 model [*Fretwell et al.*, 2013]. (inset) Outline of Antarctica, where the blue line separates East and West Antarctica (EA and WA). The red box highlights the study area.

northeast of Mt. Melbourne, surface wave analyses [*Graw et al.*, 2016] indicate that the low velocities are concentrated at shallower depths, primarily above ~100 km, and that they extend along the Ross Sea coastline. The slow seismic velocities have been interpreted as a zone of focused Cenozoic extension and rift-related decompression melting [*Graw et al.*, 2016], also consistent with the flexural uplift model for the TAMs [*Stern and ten Brink*, 1989; *ten Brink et al.*, 1997].

2.2. Anisotropy Investigations

Seismic anisotropy studies in the central and northern TAMs have been sparse and have primarily been conducted using data from the TAMSEIS array [*Lawrence et al.*, 2006b; *Barklage et al.*, 2009]. *Lawrence et al.* [2006b] estimated the anisotropic structure beneath the intersection between the N-S and E-W TAMSEIS transects (Figure 2) as part of their Rayleigh wave phase velocity analysis, where they examined periods between 20 and 120 s, which are sensitive to depths of about 30–160 km. They found φ ranging from 55° to 85° (NE-SW) with a maximum azimuthal anisotropy of 3.2 ± 1% at 40 s period, and they suggested that the observed anisotropy is constrained to the upper mantle. *Lawrence et al.* [2006b] interpret the seismic anisotropy in their study area as resulting from LPO "frozen" within the lithosphere and attribute it to past tectonic episodes, such as the Ross Orogeny (~500 Ma). *Barklage et al.* [2009] instead estimated anisotropic parameters from the splitting of SKS and SKKS phases, again recorded by TAMSEIS. Stations within the TAMs and just behind the TAMs front display an average φ of 48 ± 10°, with an average δt of 0.88 ± 0.16 s.

For stations MINN, DIHI, CCRI, SBA, and CASE (Figure 2), which are located near Ross Island and along the Ross Sea coastline, they found an average φ of 67 $\pm$ 2.3° with an average δt of 0.84 $\pm$ 0.09 s. Based on the *Lawrence et al*. [2006b] results, *Barklage et al*. [2009] estimate an azimuthal anisotropy for the central TAMs region of 3%, indicating a 150 km thick anisotropic layer, and they interpret the anisotropic signature in East Antarctica as relict upper mantle fabric predating the Ross Orogeny (~500 Ma). They further interpret the anisotropic signature near Ross Island and along the coast as possibly resulting from upper mantle flow associated with either Cenozoic-aged extension in the region or from edge-driven convection, created by the juxtaposition of the thick East Antarctic lithosphere with the thin lithosphere beneath West Antarctica.

Further to the north, only a small number of anisotropic measurements have been made throughout Northern Victoria Land, based on several seismic arrays with limited coverage. *Pondrelli et al*. [2005] and *Salimbeni et al*. [2010] examined seismic anisotropy via shear-wave splitting near Mt. Melbourne and David Glacier, respectively (Figure 1). Their results indicate a dominant NE-SW oriented φ across their respective study areas, and they note that this φ matches the tectonic trend of the TAMs, implying a correlation between the structure of the mountain range and the measured anisotropy. However, both studies also report several measurements with E-W to NNW-SSE oriented φ at specific stations, and they suggest that this variable φ may be caused by a two-layer anisotropic subsurface. The interpretation of this variable structure differs between the two studies. For instance, *Pondrelli et al*. [2005] interpret their E-W/NNW-SSE oriented φ measurements as resulting from extension during the opening of the Ross Sea, while *Salimbeni et al*. [2010] argue that these φ measurements mirror tectonic structures associated with the Ross Orogeny. The δt estimates also differ between these studies. *Pondrelli et al*. [2005] found an average δt of 1.6 s associated with their dominant φ, suggesting an anisotropic layer beneath their study area that may be thick and deeply rooted. *Salimbeni et al*. [2010], on the other hand, indicate a faster average δt (~2 s) associated with their dominant NE-SW oriented φ. Further, for stations displaying E-W/NNW-SSE oriented φ, *Salimbeni et al*. [2010] suggest δt values ranging from 0.9 to 2.3 s for a lower layer of anisotropy and from 0.9 to 2.9 s for an upper layer of anisotropy, again based on a two-layer anisotropic model. From these estimates, they calculate an anisotropic thicknesses beneath David Glacier ranging from 270 to 675 km. Since average lithospheric thickness beneath East Antarctica is ~250 km [*Morelli and Danesi*, 2004], this places the anisotropic layers below the lithosphere; therefore, *Salimbeni et al*. [2010] conclude that anisotropy beneath the David Glacier region must have an asthenospheric contribution.

3. Data and Methods

To expand the investigations of seismic anisotropy in the northern TAMs, we employ data recorded by the TAMNNET array, which consisted of 15 polar-rated broadband seismometers deployed in a previously unexplored area of Northern Victoria Land (Figure 2) [*Hansen et al*., 2015]. Ten TAMNNET stations were deployed along a linear transect, with roughly 30 km spacing, extending from the Ross Sea coast inland across the TAMs. The remaining five stations were situated on the East Antarctic ice sheet behind the TAMs front. The southernmost station (KNYN) reoccupies a station site from the previous TAMSEIS array (E030; Figure 2). TAMNNET operated from November 2012 until its decommission in December 2015 and collected data year round.

The events used in this study have epicentral distances of 90–140°, with a minimum moment magnitude of 5.8, and a total of 51 events were used for shear-wave splitting analysis (Figure 3). Azimuthal event coverage is primarily to the NW-N and SE of the TAMNNET array. PKS, SKS, and SKKS phases from these events were employed and were assessed based on their signal-to-noise ratios and their distinction from other phases. These three phases were chosen because they have a near-vertical incidence angle beneath the examined stations and, more importantly, result from a *P*-to-*S* conversion at the core-mantle boundary, which creates an *S* wave with purely *SV* polarization. Such polarization is advantageous because the waveform will not have a corresponding *SH* component after conversion. This means that any splitting of the *SV* wave as it passes through anisotropic material, thereby generating an *SH* component, must occur between the core-mantle boundary and the surface. Of the 51 examined events, the data yielded 4 individual PKS measurements, 89 individual SKS measurements, and 57 individual SKKS measurements (supporting information Table S1). Prior to analysis, the data were band-pass filtered with corner frequencies ranging from 0.01–0.02 to 0.1–0.5 Hz. These filters were not phase-specific as the data are generally noisy, and different event-station pairs required different filters to make adequate splitting measurements (supporting information

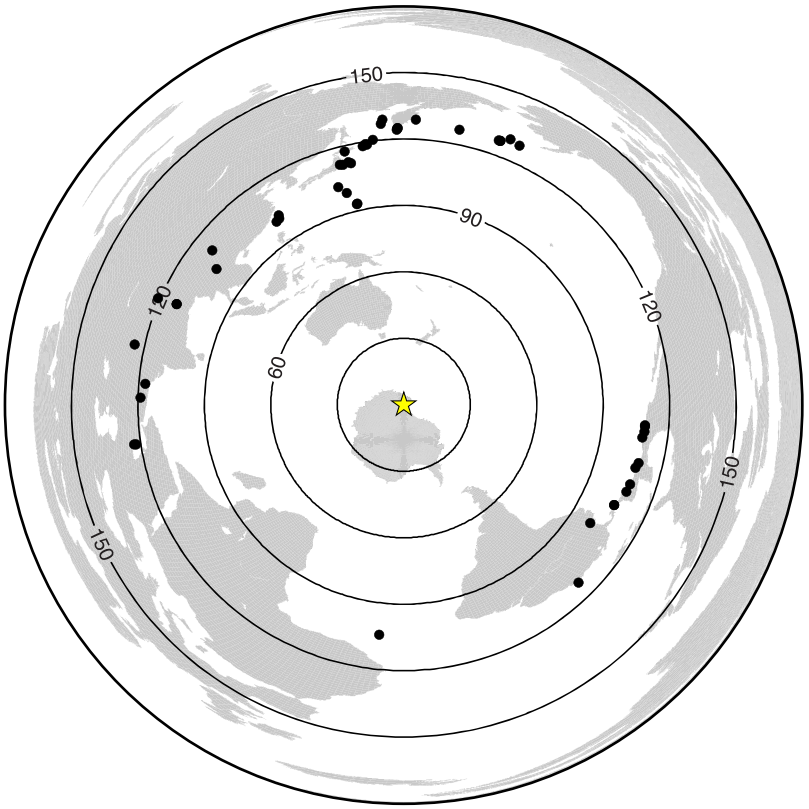

Figure 3. Map showing the locations for each of the 51 events (black dots) used in this study. The yellow star marks the center of the TAMNNET array. Events lie within an epicentral distance of 90–140°. Concentric circles mark epicentral distance from the center of the array in 30° increments. Note the event gaps to the NE and S-SW.

Table S1). Stations located near the Ross Sea coastline and within the TAMs were generally noisier than those behind the TAMs front. Therefore, band-pass filtering for these stations was primarily performed with corner frequencies of 0.01–0.1 Hz, though in some instances, slightly higher corner frequencies (0.02–0.2 Hz) were used instead. Behind the TAMs front, filtering limits of 0.02–0.2 or 0.02–0.3 Hz were generally applied. We found no correlation between the filtering limits and event magnitude; rather, the quality of the data dictated what filtering was applied. Since the corner frequencies were only varied by a small amount, there was no significant variation to the resulting φ and δt measurements described below.

We measure seismic anisotropy using the MATLAB-based SplitLab software package [*Wüstefeld et al*., 2008]. The anisotropic parameters (φ, δt) are estimated using the eigenvalue technique [*Silver and Chan*, 1991]. The eigenvalue computation calculates covariance matrices of the seismograms for different φ and δt values, which are representations of particle motion linearity. In order to quantify more linear particle motion, minimization of the smaller eigenvalue magnitude is performed, thereby removing the effects of anisotropy and determining the most appropriate φ and δt. An example is shown in Figure 4.

Individual splitting measurements for a given event-station pair have been rated as good, fair, or poor based on three criteria: (1) the measurement had a signal-to-noise ratio greater than 4, (2) the measurement resulted in linear particle motion after correcting for the splitting, and (3) there is coherence between the fast and slow *S* waves. A measurement was given a good rating if it satisfied all three criteria, a rating of fair if it satisfied two criteria, and a rating of poor if it only satisfied one criterion. This rating serves as a quality check for individual measurements, and only those with a good or fair rating were used for interpretation (Figure 5). Null measurements were assigned to observations that displayed no energy on the transverse component and are not used for further analysis in this study. All measurements are summarized in supporting information Table S1.

Some seismic anisotropy studies, both in Antarctica and elsewhere in the world, have investigated the possibility of multiple anisotropic layers in the subsurface [e.g., *Silver and Savage*, 1994; *Barklage et al*., 2009; *Salimbeni et al*., 2010]. For the examined seismic phases, the initial polarization direction aligns with the

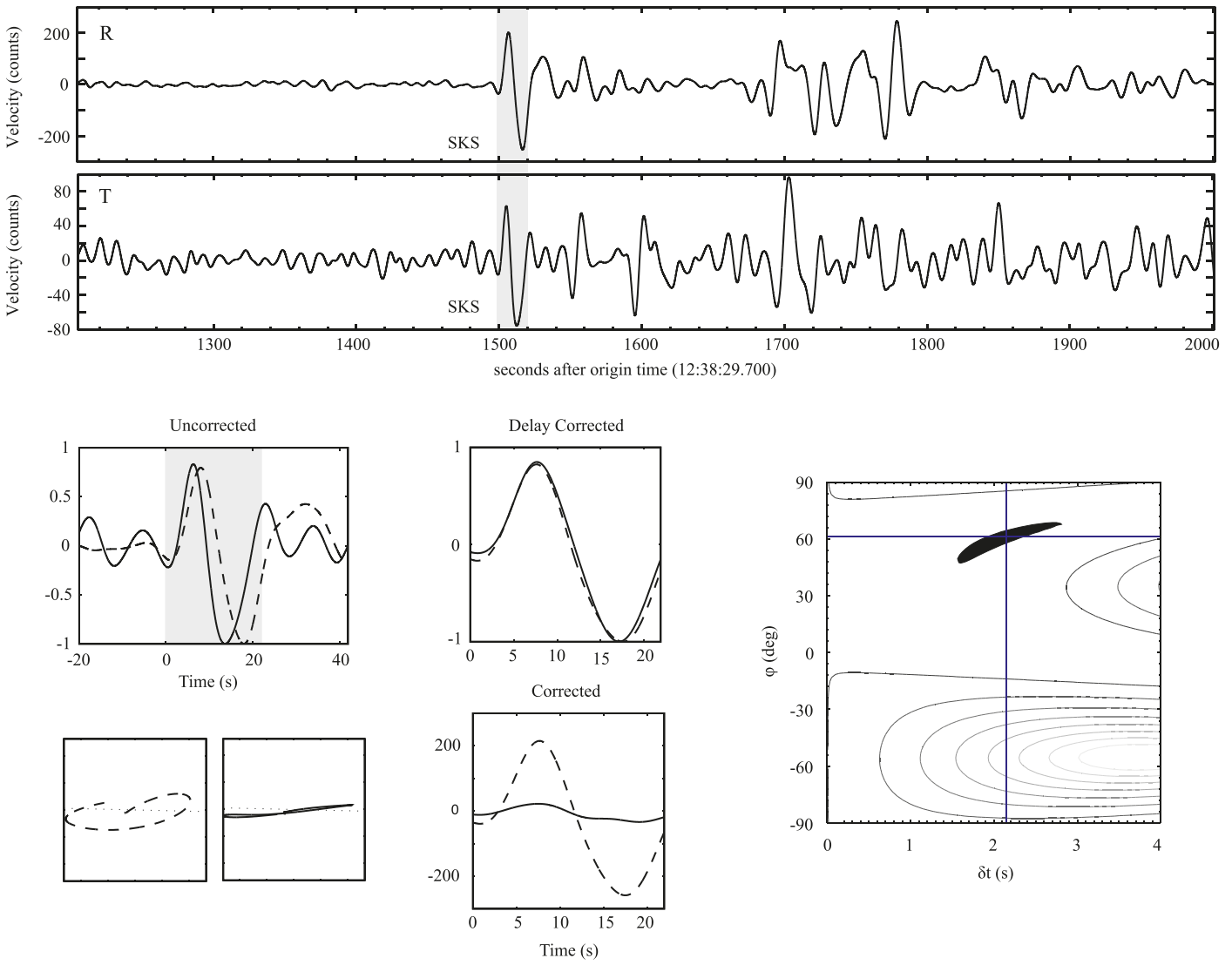

Figure 4. An example of the shear-wave splitting analysis from station MICH, using a magnitude 6.2 earthquake from 21 August 2013. (top) Original waveforms rotated into their respective radial (R) and transverse (T) components. The windowed SKS phase is highlighted in grey. (bottom left) A zoomed image of the SKS phase before analysis, with the fast and slow components indicated by the solid and dashed lines, respectively. The particle motion plots below the SKS plot indicate elliptical particle motion before correcting for the splitting (left) and linear particle motion once the splitting has been removed (right). (bottom middle) Time delay (δt) corrected radial and transverse components (upper plot) and both components corrected for splitting (lower plot). (bottom right). A misfit (error) contour plot with respect to the measured anisotropic parameters (i.e., φ and δt). Results from this example were given a "good" rating, as described in the text.

back-azimuth direction due to the conversion from *P* to *SV* as the phase leaves the outer core. If two or more anisotropic layers are present, the splitting parameters (φ, δt) will display a quasi-90° pattern when plotted as a function of back-azimuth (or initial polarization) [*Silver and Savage*, 1994; *Wüstefeld et al*., 2008]. We consider such multilayer structure when analyzing our data; however, due to large azimuthal gaps in our data set (Figure 3), we are unable to definitively assess the existence of multiple layer anisotropy. Therefore, we interpret our results as occurring from a single anisotropic layer since this is the simplest model that adequately fits the data. Using the good-rated and fair-rated splitting estimates described above (Figure 5), an average φ and δt are computed for each station. Standard error estimates are also computed for each station, for both the average φ and δt, based on the individual measurements (Table 1; supporting information Text S1).

4. Results

Generally, our results show an average φ oriented at 44 $\pm$ 2° across the entire study area, with a corresponding average δt of 1.0 $\pm$ 0.08 s (Table 1 and Figure 6). Only one splitting measurement could be made at

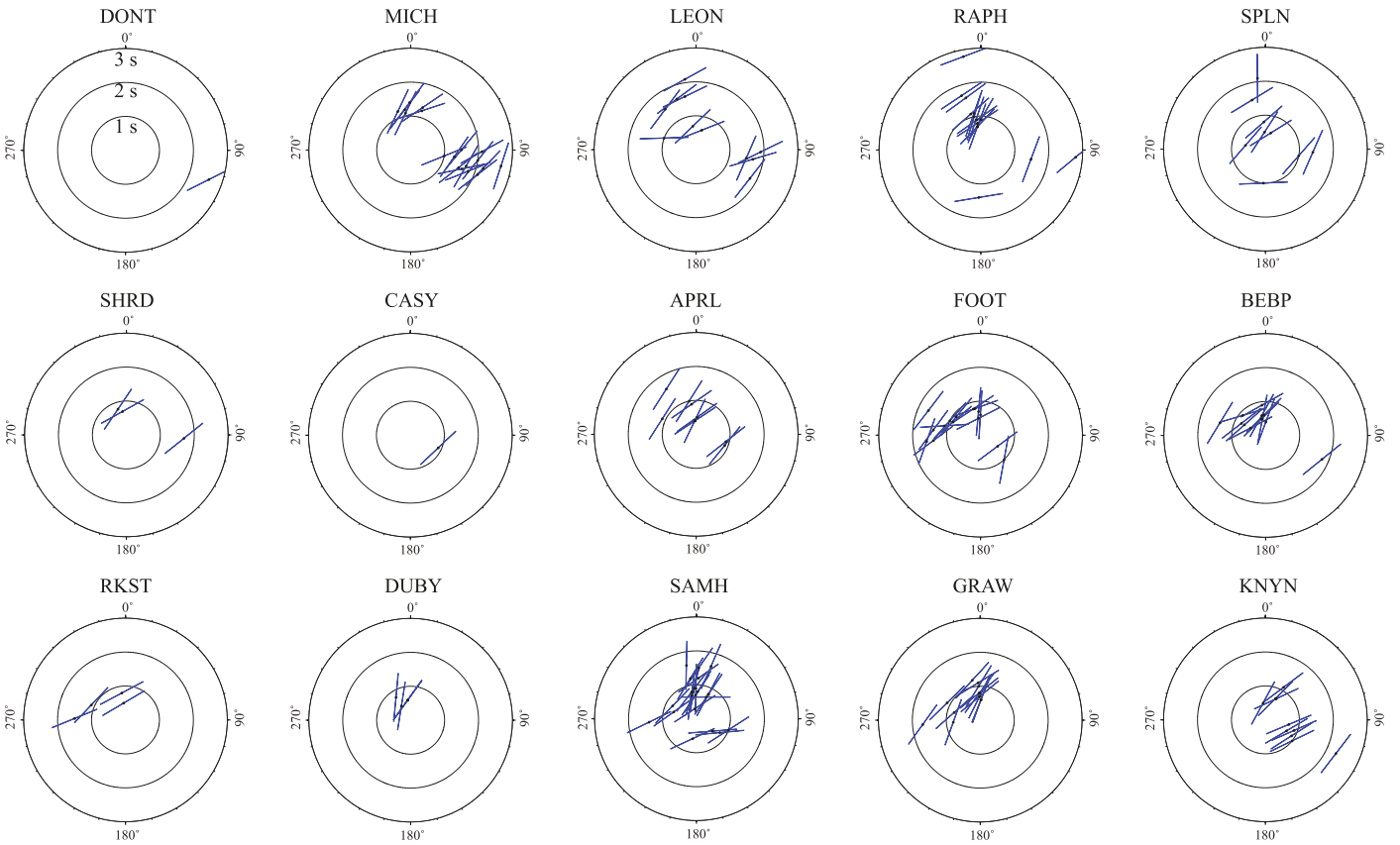

Figure 5. Shear-wave splitting results for each TAMNNET station. All measurements shown have either a good or fair rating (see text for details). Concentric circles indicate the δt (1–3 s) and vectors align with the φ. Averages of these measurements are summarized in Table 1.

stations DONT and CASY (Table 1; Figures 2 and 5); hence, we do not include these stations in further analysis or interpretation. To further assess our results, we perform a *t* test to determine if the φ and/or δt are statistically different from station to station (see supporting information Tables S2 and S3). The *t* test is performed with a 95% confidence interval, and we interpret significance based on the *t* value being lower than its respective threshold. The *t* value calculated for each station was compared to those computed at every other station to assess whether different regional areas of anisotropy exist. The corresponding results from the statistical *t* test show that there is no significant difference in the measured φ across the TAMNNET array. However, two statistically different groups are identified based on differences in the δt. Stations MICH

Table 1. Average Shear-Wave Splitting Results for Each TAMNNET Station[a]

Station	Latitude (°)	Longitude (°)	φ (°)	Eφ (+/−)	δt (s)	Eδt (+/−)	No. of Obs.
DONT	−73.87	165.12	63		2.60		1
MICH	−73.81	164.09	46	3	1.60	0.118	18
LEON	−73.71	163.32	56	5	1.45	0.085	11
RAPH	−73.54	162.28	42	4	1.32	0.175	15
SPLN	−73.46	161.47	45	6	1.00	0.161	10
SHRD	−73.39	160.49	48	5	1.06	0.287	3
CASY	−73.29	159.63	46		0.90		1
APRL	−73.19	158.70	42	5	0.85	0.127	9
FOOT	−73.09	157.85	41	5	1.00	0.107	15
BEBP	−73.03	156.86	44	6	0.80	0.096	12
RKST	−74.20	159.00	58	5	0.97	0.195	4
DUBY	−74.98	158.07	21	5	0.62	0.061	4
SAMH	−75.20	153.99	41	4	0.92	0.077	23
GRAW	−74.00	154.98	37	2	0.91	0.079	13
KNYN	−76.23	153.32	52	4	0.92	0.157	11

[a]Fast axis direction is denoted as φ and delay time is denoted as δt. Eφ and Eδt are the standard error calculations for a given station.

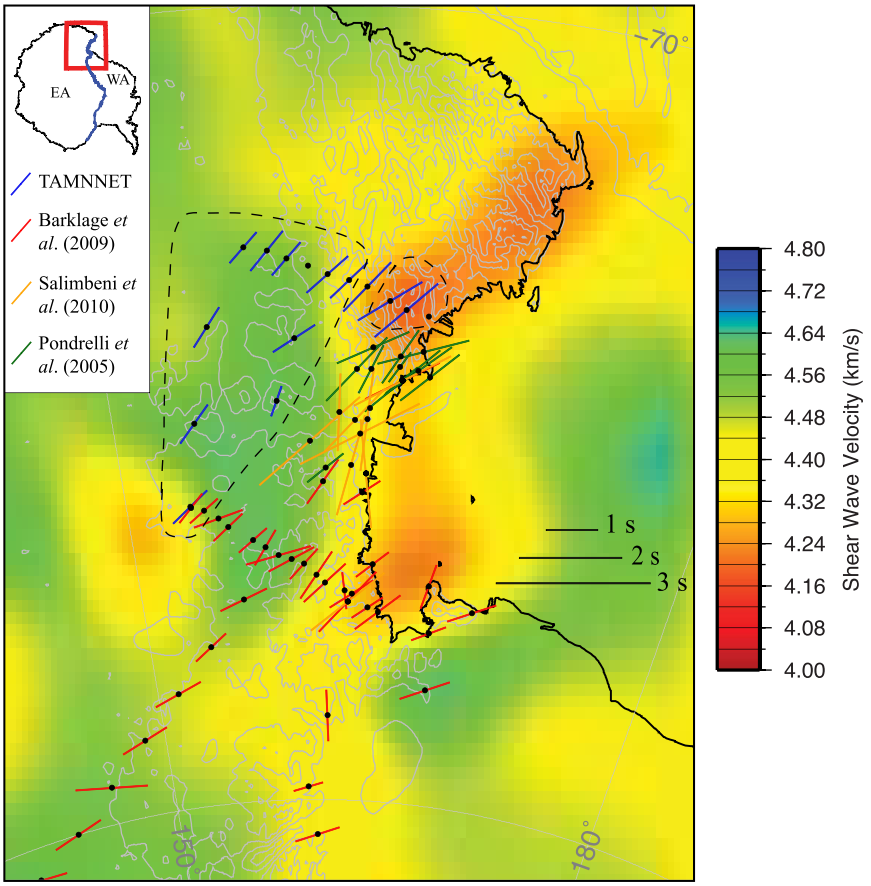

Figure 6. Anisotropic results throughout the study area, in relation to upper mantle tomography. At each station (black dots), the line is oriented in the direction of φ and its length is scaled to δt (see scale on the right side of the map). Blue lines represent results from this study (TAMNNET), red lines are results from *Barklage et al.* [2009], orange lines are results from *Salimbeni et al.* [2010], and green lines are results from *Pondrelli et al.* [2005]. Dashed enclosures highlight the two distinct zones of anisotropy as defined by our *t* test results. The tomographic image is the shear-wave velocity structure at 100 km depth from *Graw et al.* [2016]. Grey lines are the same bedrock topography contours shown in Figures 1 and 2.

and LEON, which are located near the Ross Sea coastline (Figures 2 and 6), have δt that are statistically the same as each other but which differ from most of the remaining stations and hence, form their own statistically significant group. For further discussion, we will refer to stations MICH and LEON as the coastal stations, while most of the remaining stations will be referred to as the East Antarctic stations. One notable exception is station RAPH (Figures 2 and 6), which has a δt that could be statistically joined with either group. That is, it is statistically the same as both the coastal and the East Antarctic stations. Therefore, station RAPH is interpreted as marking the boundary between the two identified groups.

A direct comparison to previous TAMSEIS anisotropy measurements can be made with station KNYN (Figure 2), as both the TAMNNET and TAMSEIS networks occupied this same site. Our results indicate a φ of 52 $\pm$ 4° and a δt of 0.92 $\pm$ 0.16 s, while *Barklage et al.* [2009] report a φ oriented at 44 $\pm$ 7° and a δt of 0.7 $\pm$ 0.1 s. These estimates agree within their respective uncertainty measurements. More broadly, our East Antarctic stations display an average φ of 42° $\pm$ 3° and have an average δt of 0.9 $\pm$ 0.04 s (Table 1 and Figure 6). For stations along and behind the TAMs front, *Barklage et al.* [2009] reported an average φ of 48 $\pm$ 10° and an average δt of 0.88 $\pm$ 0.16 s (Figure 6). Again, these estimates are similar to our findings.

Our coastal stations show an average φ of 51 $\pm$ 5°. This orientation appears to be rotated somewhat further clockwise compared to the East Antarctic stations; however, our *t* test analyses indicate that φ is statistically the same for both regions. On the other hand, δt for the coastal stations averages 1.5 $\pm$ 0.08 s, which is significantly larger than the average δt for the East Antarctic stations (0.9 $\pm$ 0.04 s). Splitting measurements for our coastal stations well match those from *Pondrelli et al.* [2005] and *Salimbeni et al.* [2010], who found

dominantly NE-SW oriented φ, with an average δt of 1.67 s. These studies examined areas only 85–180 km away from our coastal sites (Figure 6). As noted in section 2.2, *Pondrelli et al*. [2005] and *Salimbeni et al*. [2010] also report that some of their stations display more E-W to NNW-SSE oriented φ, but we did not find any φ measurements with such azimuths. Our measured φ generally follow the trend of the TAMs inside the bend of Northern Victoria Land, toward the northeast (Figure 6).

5. Discussion

5.1. Depth Extent of Anisotropy

Shallow sources of anisotropy may result from ice and crustal layers beneath a given station. Ice is a highly anisotropic material, with φ typically oriented in the direction of ice flow. *Thiel and Ostenso* [1961], for instance, found that changes in shear-wave velocity passing through an ice crystal are on the order of 5%. Since all of the TAMNNET stations were installed on ice (ranging from 0.1 to 2.9 km in thickness), anisotropy from the ice layer could contribute to our observations. However, even for a 3 km thick ice layer, the corresponding δt would be $\sim$0.1 s, which is much less than our determined δt values of 0.9 ± 0.04 and 1.5 ± 0.08 s for the East Antarctic and coastal stations, respectively. In the crust, typical azimuthal anisotropy is 2–4% [*Babuska and Cara*, 1991; *Barruol and Mainprice*, 1993]. Assuming an average crustal thickness of 40 km beneath TAMNNET [*Hansen et al*., 2016], a δt of 0.2–0.4 s would be expected. This is in good agreement with crustal δt estimates (0.05–0.2 s) provided by *Savage* [1999]; however, this is again much lower than our observed δt across the study area.

While we cannot completely dismiss ice and crustal influence on our anisotropic measurements, we find that the corresponding δt associated with these layers is too small to explain our results. This conclusion is supported by *Savage* [1999], who indicated that splitting times greater than 0.2–0.3 s are typically representative of upper mantle anisotropy. Constraints on the depth of anisotropy within the mantle are debated; however, it is suggested that most anisotropy is confined to the upper 200–300 km [e.g., *Nishimura and Forsyth*, 1988; *Gaherty et al*., 1996]. *Savage* [1999], for instance, showed that δt values within the upper mantle could be as high as 3.0 s, while δt values within the lower mantle are generally $<$0.2 s. Therefore, we turn our attention from near-surface and crustal sources to upper mantle sources of anisotropy to interpret our findings.

5.2. Anisotropy in East Antarctica

To estimate the thickness of an anisotropic layer, the azimuthal anisotropy percentage (or magnitude) must be known. As stated in section 2.2, *Lawrence et al*. [2006b] estimated the anisotropy within the central TAMs at $\sim$3%, based on their results using Rayleigh wave phase velocities. It should be noted that *Lawrence et al*. [2006b] obtained their azimuthal anisotropy estimate from horizontally propagating waves, yielding an apparent measurement of anisotropy. Vertically propagating waves, such as PKS, SKS, and SKKS, may have a different maximum azimuthal anisotropy. For example, depending on the orientation of olivine assemblages in the subsurface, horizontally and vertically propagating waves could display a maximum azimuthal anisotropy that differ from each other by $\sim$2% [e.g., *Tommasi et al*., 1999]. *Barklage et al*. [2009] estimated splitting parameters for TAMSEIS stations behind the TAMs front that are congruent with our estimates for the TAMNNET East Antarctic stations (Figure 6), and they also suggested a continuance of their interpreted anisotropic structure to the north, toward the Wilkes Subglacial Basin (Figure 1). Based on results from *Lawrence et al*. [2006b], *Barklage et al*. [2009] assumed 3% anisotropy within East Antarctica; therefore, we use this same percentage, but we also include a range of conservative azimuthal anisotropy percentages, up to 5%, in our estimations of anisotropic layer thickness. This 3-5% range takes into account any apparent azimuthal anisotropy variations resulting from mineral alignment in the subsurface. The average δt of 0.9 ± 0.04 s for the East Antarctic stations suggests an 81–135 km thick anisotropic layer. Since we do not consider an influence from either the ice or the crust, this indicates that the anisotropic layer could extend from 42 to 177 km depth behind the northern TAMs front. Global-scale and continental-scale [*Danesi and Morelli*, 2001; *Ritzwoller et al*., 2001; *Morelli and Danesi*, 2004; *Hansen et al*., 2014] as well as regional-scale [*Graw et al*., 2016; *Brenn*, 2016] tomographic images show fast compressional and shear-wave velocities down to at least 200 km depth beneath this region, indicative of cratonic lithosphere. This is corroborated by results from *Morelli and Danesi* [2004], who suggest an average lithospheric thickness beneath East Antarctica of $\sim$250 km. An anisotropic layer contained within the continental lithosphere eliminates active

upper mantle flow as a source, and thus must reflect LPO structure "frozen" into the lithosphere from previous tectonic events [*Babuska and Plomerova*, 2006].

Stations within the TAMs and those further inland all display a statistically similar anisotropic signature (Figure 6); therefore, the origin of the "frozen" anisotropy must be the same. That is, the anisotropy cannot be tied to the origin of the TAMs since the same characteristics are also observed within East Antarctica. Therefore, to further assess the relict anisotropic fabric affecting these stations, we must consider the tectonic history of this portion of our study region. As discussed in section 1.0, East Antarctica has experienced a number of mountain building events during its geologic past, and observed anisotropy associated with mountain building characteristically has φ oriented orthogonal to the direction of compression [*Vinnik et al*., 1992]. The Ross Orogeny was one of the largest compressional tectonic events affecting our study area, occurring at ~500 Ma. Evidence for the Ross Orogeny from exposed bedrock in the TAMs indicates structures and fabrics with NW-SE orientations [*Findlay*, 1978, 1984; *Allibone*, 1987; *Stump*, 1995]. Such structural trends suggest a NE-SW direction of shortening, which would result in a NW-SE seismically oriented φ. This is inconsistent with the results from our study, which instead show φ oriented NE-SW, thereby indicating that the Ross Orogeny cannot be correlated to our observed anisotropy behind the TAMs front.

The Beardmore (~625 Ma) and Nimrod (~1.7 Ga) Orogenies predate the Ross Orogeny and also significantly affected our study area. Evidence for these earlier tectonic events can be found within the lithology of exposed outcrops within the TAMs, particularly within the southern Ross Ice Shelf area, where the Nimrod Group is located. The Nimrod Group exhibits ductile tectonic fabrics, which are correlated to midcrustal Ross deformation; however, U-Pb zircon age data from meta-igneous and gneissic rocks of the Nimrod Group reflect a period of magmatism and deep-crustal metamorphism occurring ~1725 Ma [*Goodge et al*., 2001]. These data suggest that the area experienced intense tectonic collision during this time, which has been proposed as the Nimrod Orogeny. Similar geochemical signatures are found in surrounding outcrops, with additional age data marking a collisional event near the end of the Proterozoic, which has been associated with the Beardmore Orogeny [*Stump et al*., 1986]. It has been suggested that large degrees of tectonic over-printing by later events, such as the Ross Orogeny, have erased much of the structural evidence from the Nimrod and Beardmore Orogenies [*Grindley and McDougall*, 1969; *Goodge et al*., 2001]. Nonetheless, these past tectonic episodes could likely be the source(s) of anisotropy behind the TAMs front. *Barklage et al*. [2009] made similar conclusions. We extrapolate their interpretation to the north and also suggest that seismic anisotropy behind the northern TAMs is associated with ancient deformational episodes predating the Ross event.

5.3. Anisotropy Along the Ross Sea Coastline

The coastal stations show statistically different δt (1.5 ± 0.08 s) from the East Antarctic stations (0.9 ± 0.04 s). As mentioned previously, δt depends on the thickness of an anisotropic layer as well as the percentage or magnitude of anisotropy within that layer. Typically, azimuthal anisotropy in the upper mantle averages ~3.7% [*Mainprice and Silver*, 1993]. However, results from previous seismological investigations within our study area indicate various upper mantle anomalies, such as slow seismic velocities along the Ross Sea coastline [*Graw et al*., 2016; *Brenn*, 2016], thin lithosphere beneath the adjacent WARS (~60–80 km) [*Huerta*, 2007; *Huerta and Harry*, 2007], and increased anisotropic delay times near David Glacier and Mt. Melbourne [*Pondrelli et al*., 2005; *Salimbeni et al*., 2010]. Therefore, given this variability, we conservatively use magnitudes ranging from % to 5% to estimate the anisotropic layer thickness. With an average δt of 1.5 ± 0.08 s for the coastal stations, the corresponding anisotropic layer thickness ranges from 135 to 225 km. Further, assuming an average crustal thickness of ~38 km beneath the coastal stations, as suggested by *Hansen et al*. [2016], the anisotropic layer could extend roughly from 39 to 264 km in the upper mantle. Unlike the East Antarctic stations, where the anisotropic signature appears to be concentrated in the cratonic lithosphere, the depth extent of the anisotropic signature along the Ross Sea coastline constrains the anisotropy within the lower-viscosity, higher-temperature asthenosphere. Therefore, the observed anisotropy has strong implications for understanding the current dynamic state of the mantle beneath the eastern portion of our study area.

As discussed in section 1.0, seismic anisotropy can result from active mantle flow, creating LPO in the dominant flow direction. In some cases, such LPO may be induced by the motion of a tectonic plate, where the underlying asthenospheric material is pulled in the direction of APM by the rigid overlying lithosphere,

ultimately leading to φ oriented parallel to the direction of plate motion [*Wolfe and Silver*, 1998]. Our results are inconsistent with this mechanism, as APM in the Ross Sea region is oriented at ~342° [*Gripp and Gordon*, 2002], while our results indicate φ oriented at 51 ± 5°. Additionally, seismic anisotropy associated with APM requires relatively fast plate velocities [*Bokelmann and Silver*, 2002], but the average APM velocity in the Ross Sea region is quite slow, averaging ~1.5 cm yr^{-1} [*Gripp and Gordon*, 2002]. Given the large difference between the observed φ and APM (~67°) as well as the slow APM rate, it is unlikely that the anisotropic signature we observe along the Ross Sea coast results from APM-induced mantle flow.

Alternatively, seismic anisotropy can also result from mantle flow associated with tectonic processes and active deformation, where the LPO of olivine aligns parallel to the dominant flow direction [*Ribe*, 1989]. Comparing our anisotropy results for the coastal stations with regional TAMNNET tomographic studies [*Graw et al*., 2016; *Brenn*, 2016], it is interesting that the inferred anisotropic layer thickness (135–225 km) well matches the ~180 km depth extent of prominent, slow upper mantle velocities imaged beneath the Ross Sea coastline and the northern TAMs. These low velocities have been interpreted to reflect rift-related decompression melting and Cenozoic extension focused along a narrow zone adjacent to the central and northern TAMs, known as the Terror Rift (Figure 1). The slow seismic signature extends laterally beneath the northern TAMs front, terminating beneath station RAPH (Figures 2 and 6) [*Graw et al*., 2016; *Brenn*, 2016], which coincidentally, is the boundary station between our two distinct zones of anisotropy (see section 4.0). Further, *Graw et al*. [2016] show the low velocities extending northward beneath Victoria Land, originating at ~160 km depth beneath Mt. Melbourne and shallowing to depths of ~100 km north of the TAMNNET array (Figure 6).

Using an average, global-scale seismic velocity model [*Becker and Boschi*, 2002], *Faccenna et al*. [2008] suggested that mantle flow beneath the Victoria Land region is oriented primarily in an east-west direction. However, a combination of the higher-resolution, regional TAMNNET tomographic images [*Graw et al*., 2016; *Brenn*, 2016] with our current anisotropy results would indicate otherwise. We suggest that mantle flow beneath the northern TAMs originates from a zone of focused decompression melting at the northern end of Terror Rift. Given the low velocity structure imaged by *Graw et al*. [2016] (Figure 6), it appears that partially molten mantle migrates from Mt. Melbourne northeastward beneath northern Victoria Land, parallel to the Ross Sea coastline. This would result in a NE-SW oriented φ, following the path of the mantle flow, and this orientation matches our results well. It is worth noting that our *t* test results indicate that all the examined stations have statistically similar φ. While this could simply be a coincidence, suggesting that active upper mantle flow along the coast is oriented in the same direction as the relict fabric orientation behind the TAMs front, it may also reflect an ancient fabric orientation that is influencing the direction of the asthenospheric flow. In addition, as outlined above, the depth extent of the imaged low velocity anomaly also well matches that expected for the observed δt in this area. Therefore, we interpret the seismic anisotropic signature of our coastal stations as reflecting present-day, active upper mantle flow, previously imaged by TAMNNET tomographic studies and associated with local tectonic processes beneath the northern TAMs.

6. Summary

We find evidence for two distinct regions of anisotropy beneath the TAMNNET array in northern Victoria Land. Shear-wave splitting analyses in East Antarctica show an average φ oriented at 42 ± 3° with an average δt of 0.9 ± 0.04 s. Assuming an azimuthal anisotropy percentage ranging from 3% to 5%, consistent with previous studies [e.g., *Lawrence et al*., 2006b], this δt suggests an anisotropic layer that is 81–135 km thick and which is located within the continental lithosphere. We attribute the observed anisotropy in this area to relict fabric "frozen" into the lithosphere within East Antarctica, possibly reflecting tectonic processes predating the Ross Orogeny (~500 Ma). Coastal TAMNNET stations show an average φ of 51 ± 5°, with a statistically significant and larger average δt of 1.5 ± 0.08 s. Previous seismological studies using surface and body wave tomography [*Graw et al*., 2016; *Brenn*, 2016] indicate a prominent low velocity anomaly beneath the northern TAMs front, that extends northward from Mt. Melbourne beneath northern Victoria Land and parallel to the Ross Sea coastline. This anomaly likely serves as the source for the observed coastal anisotropy. Again, assuming conservative anisotropic percentages (3–5%), the observed δt can be explained by a 135–225 km thick anisotropic layer, which well matches the estimated depth extent (~180 km) of the slow

upper mantle anomaly. Further, the predicted mantle flow direction inferred from the tomographic images matches the observed φ orientation. Therefore, we interpret the observed anisotropy at the coastal TAMNNET stations as reflecting active upper mantle flow beneath the northern TAMs, caused by rift-related decompression melting and Cenozoic extension.

Acknowledgments
We thank the TAMNNET field team responsible for maintaining the instrumentation and for collecting the data used in this study as well as the staff at IRIS-PASSCAL, Ken Borek Air, and McMurdo Station for their logistical and technical support. We also thank Lucia Margheriti and Mickaël Bonnin for their constructive comments and critiques that greatly improved this manuscript. Data management handling and archival were provided by the IRIS-DMC. Data are currently under embargo but will become publicly available at the end of 2017. The project's DOI is http://www.fdsn.org/networks/detail/ZJ_2012/. The facilities of the IRIS Consortium are supported by the National Science Foundation (NSF) under cooperative agreement EAR-1063471, the NSF Office of Polar Programs, and the Department of Energy National Nuclear Security Administration. Funding for this research was provided by the NSF (grant ANT-1148982).

References

Allibone, A. (1987), Koettlitz Group metasediments and orthogneisses from the mid Taylor Valley and Ferrar Glacier areas, *N. Z. Antarct. Rec.*, *8*, 48–60.
Babuska, V., and M. Cara (1991), *Seismic Anisotropy in the Earth*, Kluwer, Dordrecht, The Netherlands.
Babuska, V., and J. Plomerova (2006), European mantle lithosphere assembled from rigid microplates with inherited seismic anisotropy, *Phys. Earth Planet. Inter.*, *158*, 264–280.
Barklage, M., D. A. Wiens, A. Nyblade, and S. Anandakrishnan (2009), Upper mantle seismic anisotropy of South Victoria Land and the Ross Sea coast, Antarctica from SKS and SKKS splitting analysis, *Geophys. J. Int.*, *178*, 729–741.
Barrett, P. J. (1991), The Devonian to Jurassic Beacon Supergroup of the Transantarctic Mountains and correlatives in other parts of Antarctica, in *The Geology of Antarctica*, edited by R. J. Tingey, pp. 120–152, Clarendon, Oxford, U. K.
Barruol, G., and D. Mainprice (1993), A quantitative evaluation of the contribution of crustal rocks to the shear wave splitting of teleseismic SKS waves, *Phys. Earth Planet. Inter.*, *78*, 281–300.
Becker, T., and L. Boschi (2002), A comparison of tomographic and geodynamic mantle models, *Geochem. Geophys. Geosyst.*, *3*(1), 1003, doi:10.1029/2001GC000168.
Bialas, R. W., W. R. Buck, M. Studinger, and P. G. Fitzgerald (2007), Plateau collapse model for the Transantarctic Mountains-West Antarctic Rift System: Insights from numerical experiments, *Geology*, *35*, 687–690.
Bokelmann, G. H. R., and P. G. Silver (2002), Shear stress at the base of shield lithosphere, *Geophys. Res. Lett.*, *29*(23), 2091–2095, doi:10.1029/2002GL015925.
Brenn, G. R. (2016), Determining the upper mantle seismic structure beneath the northern Transantarctic Mountains, Antarctica, from regional P- and S-wave tomography, M.S. thesis, Dep. of Geol. Sci., Univ. of Alabama, Tuscaloosa, Ala.
Chaput, J., R. C. Aster, A. Huerta, X. Sun, A. Lloyd, D. Wiens, A. Nyblade, S. Anandakrishnan, J. P. Winberry, and T. Wilson (2014), The crustal thickness of West Antarctica, *J. Geophys. Res. Solid Earth*, *119*, 378–395, doi:10.1002/2013JB010642.
Dalziel, I. W. D. (1992), Antarctica: A tale of two supercontinents?, *Annu. Rev. Earth Planet. Sci.*, *20*, 501–526.
Danesi, S., and A. Morelli (2001), Structure of the upper mantle under the Antarctic Plate from surface wave tomography, *Geophys. Res. Lett.*, *28*, 4395–4398.
Faccenna, C., F. Rossetti, T. W. Becker, S. Danesi, and A. Morelli (2008), Recent extension driven by mantle upwelling beneath the Admiralty Mountains (East Antarctica), *Tectonics*, *27*, TC4015, doi:10.1029/2007TC002197.
Findlay, R. H. (1978), Provisional report on the geology of the region between the Renegar and Blue Glaciers, Antarctica, *N. Z. Antarct. Rec.*, *1*, 39–44.
Findlay, R. H. (1984), Lithostratigraphy and structure of the Koettlitz Group, McMurdo Sound, Antarctica, *N. Z. J. Geol. Geophys.*, *27*, 513–536.
Fischer, K. M., M. J. Fouch, D. A. Wiens, and M. S. Boettcher (1998), Anisotropy and flow in Pacific subduction zone back-arcs, *Pure Appl. Geophys.*, *151*, 463–475.
Fitzgerald, P. (2002), Tectonics and landscape evolution of the Antarctic plate since the breakup of Gondwana, with an emphasis on the West Antarctic Rift System and the Transantarctic Mountains, *Bull. R. Soc. N. Z.*, *35*, 453–469.
Fitzgerald, P. G., M. Sandiford, P. J. Barrett, and A. J. W. Gleadow (1986), Asymmetric extension associated with uplift and subsidence in the Transantarctic Mountains and Ross Embayment, *Earth Planet. Sci. Lett.*, *81*, 67–78.
Fitzgerald, P. G., and E. Stump (1997), Cretaceous and Cenozoic episodic denudation of the Transantarctic Mountains, Antarctica: New constraints from apatite fission track thermochronology in the Scott Glacier region, *J. Geophys. Res.*, *102*, 7747–7765.
Fretwell, P., et al. (2013), BEDMAP2: Improved ice bed, surface and thickness datasets for Antarctica, *Cryosphere*, *7*, 375–393.
Gaherty, J. B., T. H. Jordan, and L. S. Gee (1996), Seismic structure of the upper mantle in a central Pacific corridor, *J. Geophys. Res.*, *101*, 22,291–22,309.
Goodge, J. W., C. M. Fanning, and V. C. Bennett (2001), U-Pb evidence of ~1.7 Ga crustal tectonism during the Nimrod Orogeny in the Transantarctic Mountains, Antarctica: Implications for Proterozoic plate reconstructions, *Precambrian Res.*, *112*, 261–288.
Graw, J. H., A. N. Adams, S. E. Hansen, D. A. Wiens, L. Hackworth, and Y. Park (2016), Upper mantle shear wave velocity structure beneath northern Victoria Land, Antarctica: Volcanism and uplift in the northern Transantarctic Mountains, *Earth Planet. Sci. Lett.*, *449*, 48–60.
Grindley, G. W., and I. McDougall (1969), Age and correlation of the Nimrod Group and other precambrian rock units in the central Transantarctic Mountains, Antarctica, *N. Z. J. Geol. Geophys.*, *12*, 391–411.
Gripp, A. E., and R. G. Gordon (2002), Young tracks of hotspots and current plate velocities, *Geophys. J. Int.*, *150*, 321–361.
Hansen, S. E., J. Julia, A. A. Nyblade, M. L. Pyle, D. A. Wiens, and S. Anandakrishnan (2009), Using S wave receiver functions to estimate crustal structure beneath ice sheets: An application to the Transantarctic Mountains and East Antarctic craton, *Geochem. Geophys. Geosyst.*, *10*, Q08014, doi:10.1029/2009GC002576.
Hansen, S. E., A. A. Nyblade, D. S. Heeszel, D. A. Wiens, P. Shore, and M. Kanao (2010), Crustal structure of the Gamburtsev Mountains, East Antarctica, from S-wave receiver functions and Rayleigh wave phase velocities, *Earth Planet. Sci. Lett.*, *300*, 395–401.
Hansen, S. E., J. H. Graw, L. M. Kenyon, A. A. Nyblade, D. A. Wiens, R. C. Aster, A. D. Huerta, S. Anandakrishnan, and T. Wilson (2014), Imaging the Antarctic mantle using adaptively parameterized P-wave tomography: Evidence for heterogeneous structure beneath West Antarctica, *Earth Planet. Sci. Lett.*, *408*, 66–78.
Hansen, S. E., A. M. Reusch, T. Parker, D. K. Bloomquist, P. Carpenter, J. H. Graw, and G. R. Brenn (2015), The Transantarctic Mountains Northern Network (TAMNNET): Deployment and performance of a seismic array in Antarctica, *Seismol. Res. Lett.*, *86*, 1636–1644, doi:10.1785/0220150117.
Hansen, S. E., L. M. Kenyon, J. H. Graw, Y. Park, and A. Nyblade (2016), Crustal structure beneath the Northern Transantarctic Mountains and Wilkes Subglacial Basin: Implications for tectonic origins, *J. Geophys. Res. Solid Earth*, *121*, 812–825, doi:10.1002/2015JB012325.
Heeszel, D. S., D. A. Wiens, S. Anandakrishnan, R. C. Aster, I. W. D. Dalziel, A. D. Huerta, A. A. Nyblade, T. J. Wilson, and P. Winberry (2016), Upper mantle structure of central and West Antarctica from array analysis of Rayleigh wave phase velocities, *J. Geophys. Res. Solid Earth*, *121*, 1758–1775, doi:10.1002/2015JB012616.

Huerta, A. D. (2007), Lithospheric structure across the Transantarctic Mountains constrained by an analysis of gravity and thermal structure, in *Antarctica: A Keystone in a Changing World—Online Proceedings of the 10th ISAES, USGS Open-File Rep. 2007-1047, Short Research Paper 022*, edited by A. K. Cooper et al., 4 pp., doi:10.3133/of2007-1047.srp022.

Huerta, A. D., and D. L. Harry (2007), The transition from diffuse to focused extension: Modeled evolution of the West Antarctic Rift system, *Earth Planet. Sci. Lett.*, *255*, 133–147.

Kalamarides, R. I., J. H. Berg, and R. A. Hank (1987), Lateral isotopic discontinuity in the lower crust: An example from Antarctica, *Science*, *237*, 1192–1195.

Karner, G. D., M. Studinger, and R. E. Bell (2005), Gravity anomalies of sedimentary basins and their mechanical implications: Application to the Ross Sea basins, West Antarctica, *Earth Planet. Sci. Lett.*, *235*, 577–596.

Kyle, P. R., and H. L. Muncy (1989), Geology and geochronology of McMurdo Volcanic Group rocks in the vicinity of Lake Morning, McMurdo Sound, *Antarct. Sci.*, *4*, 345–350.

Lawrence, J. F., D. A. Wiens, A. Nyblade, S. Anandakrishnan, P. J. Shore, and D. Voigt (2006a), Crust and upper mantle structure of the Transantarctic Mountains and surrounding regions from receiver functions, surface waves, and gravity: Implications for uplift models, *Geochem. Geophys. Geosyst.*, *7*, Q10011, doi:10.1029/2006GC001282.

Lawrence, J. F., D. A. Wiens, A. A. Nyblade, S. Anandakrishnan, P. J. Shore, and D. Voigt (2006b), Rayleigh wave phase velocity analysis of the Ross Sea, Transantarctic Mountains, and East Antarctica from a temporary seismograph array, *J. Geophys. Res.*, *111*, B06302, doi:10.1029/2005JB003812.

Lisker, F., and A. L. Läufer (2013), The Mesozoic Victoria Basin: Vanished link between Antarctica and Australia, *Geology*, *41*, 1043–1046.

Mainprice, D., and P. G. Silver (1993), Interpretation of SKS-waves using samples from the subcontinental lithosphere, *Phys. Earth Planet. Inter.*, *78*, 257–280.

Mainprice, D., A. Tommasi, H. Couvy, P. Cordier, and D. J. Frost (2005), Pressure sensitivity of olivine slip systems and seismic anisotropy of Earth's upper mantle, *Nature*, *433*, 731–733.

Morelli, A., and S. Danesi (2004), Seismological imaging of the Antarctic continental lithosphere: A review, *Global Planet. Change*, *42*, 155–165.

Nishimura, C. E., and D. W. Forsyth (1988), Rayleigh wave phase velocities in the Pacific with implications for azimuthal anisotropy and lateral heterogeneity, *Geophys. J. R. Astron. Soc.*, *94*, 497–501.

Pondrelli, S., L. Margheriti, and S. Danesi (2005), Seismic anisotropy beneath Northern Victoria Land from SKS splitting analysis, in *Antarctica: Contributions to Global Earth Sciences*, edited by D. K. Fütterer et al., pp. 153–160, Springer, Berlin Heidelberg, New York.

Ribe, N. M. (1989), Seismic anisotropy and mantle flow, *J. Geophys. Res.*, *94*, 4213–4223.

Ritzwoller, M. H., N. M. Shapiro, A. L. Levshin, and G. M. Leahy (2001), Crustal and upper mantle structures beneath Antarctica and surrounding oceans, *J. Geophys. Res.*, *106*, 30,645–30,670.

Robinson, E. S., and J. F. Splettstoesser (1984), Structure of the Transantarctic Mountains determined from geophysical surveys, in *Geology of the Central Transantarctic Mountains, Antarctic Res. Ser 36*, edited by M. D. Turner and J. E. Splettstoesser, pp. 119–162, American Geophysical Union, Washington, D. C.

Salimbeni, S., S. Pondrelli, S. Danesi, and A. Morelli (2010), Seismic anisotropy of the Victoria Land region, Antarctica, *Geophys. J. Int.*, *182*, 421–432.

Savage, M. K. (1999), Seismic anisotropy and mantle deformation: What have we learned from shear wave splitting?, *Rev. Geophys.*, *37*, 65–106.

Sieminski, A., E. Debayle, and J. Leveque (2003), Seismic evidence for deep low-velocity anomalies in the transition zone beneath West Antarctica, *Earth Planet. Sci. Lett.*, *216*, 645–661.

Silver, P. G., and W. W. Chan (1988), Implications for continental structure and evolution from seismic anisotropy, *Nature*, *335*, 34–39.

Silver, P. G., and W. W. Chan (1991), Shear wave splitting and subcontinental mantle deformation, *J. Geophys. Res.*, *96*, 16,429–16,454.

Silver, P. G., and M. Savage (1994), The interpretation of shear-wave splitting parameters in the presence of two anisotropic layers, *Geophys. J. Int.*, *119*, 949–963.

Stern, T. A., and U. S. ten Brink (1989), Flexural uplift of the Transantarctic Mountains, *J. Geophys. Res.*, *94*, 10,315–10,330.

Studinger, M., R. E. Bell, W. R. Buck, G. D. Karner, and D. D. Blankenship (2004), Sub-ice geology inland of the Transantarctic Mountains in light of new aerogeophysical data, *Earth Planet. Sci. Lett.*, *220*, 391–408.

Stump, E. (1995), *The Ross Orogen of the Transantarctic Mountains*, Cambridge Univ. Press, Cambridge, U. K.

Stump, E., J. H. Smit, and S. Self (1986), Timing of events during the late Proterozoic Beardmore Orogeny, Antarctica: Geologic evidence from the La Gorce Mountains, *Geol. Soc. Am. Bull.*, *97*, 953–965.

ten Brink, U. S., R. I. Hackney, S. Bannister, T. A. Stern, and Y. Makovsky (1997), Uplift of the Transantarctic Mountains and the bedrock beneath the East Antarctic ice sheet, *J. Geophys. Res.*, *102*, 27,603–27,621.

Thiel, E., and N. A. Ostenso (1961), Seismic studies on Antarctic ice shelves, *Geophysics*, *26*, 706–715.

Tommasi, A., B. Tikoff, and A. Vauchez (1999), Upper mantle tectonics: Three-dimensional deformation, olivine crystallographic fabrics and seismic properties, *Earth Planet. Sci. Lett.*, *168*, 173–186.

Vinnik, L. P., L. I. Makeyeva, A. Milev, and A. Y. Usenko (1992), Global patterns of azimuthal anisotropy and deformations in the continental mantle, *Geophys. J. Int.*, *111*, 433–447.

Watson, T., A. Nyblade, D. A. Wiens, S. Anandakrishnan, M. Benoit, P. J. Shore, D. Voigt, and J. VanDecar (2006), P and s velocity structure of the upper mantle beneath the Transantarctic Mountains, East Antarctic craton, and Ross Sea from travel time tomography, *Geochem. Geophys. Geosyst.*, *7*, Q07005, doi:10.1029/2005GC001238.

Wolfe, C. J., and P. G. Silver (1998), Seismic anisotropy of oceanic upper mantle: Shear-wave splitting methodologies and observations, *J. Geophys. Res.*, *103*, 749–771.

Wüstefeld, A., G. Bokelmann, C. Zaroli, and G. Barruol (2008), SplitLab: A shear-wave splitting environment in Matlab, *Comput. Geosci.*, *34*, 515–528.

Zhang, S., S. Karato, J. F. Gerald, U. Faul, and Y. Zhou (2000), Simple shear deformation of olivine aggregates, *Tectonophysics*, *316*, 133–152.